Meteorol. Z. (Contrib. Atm. Sci.), Early Access DOI 10.1127/metz/2023/1165

Early Access Article

Evaluating Bunkers' storm motion of hail-producing supercells and their storm-relative helicity in Germany

Mathis Tonn, Jannik Wilhelm and Michael Kunz*

Institute of Meteorology and Climate Research (IMK-TRO), Karlsruhe Institute of Technology (KIT), Karlsruhe Germany

(Manuscript received August 29, 2022; in revised form February 23, 2023; accepted April 13, 2023)

Abstract

This paper presents a statistical analysis of the motion of hail-producing supercells in Germany based on data from a radar-based cell detection and tracking algorithm and a mesocyclone detection algorithm. The parameterization of supercell motion by Bunkers et al. (2000), originally developed using storm data from the United States, is evaluated regarding its applicability in Central Europe, where storm environments have other dynamic and thermodynamic characteristics owing to different geographical features. As a first step, the motion of 354 observed supercells in the warm season (April to September) 2013–2016 is compared to the motion obtained with the original parameterization. The cells are classified as right-moving or left-moving supercells due to their motion direction with regard to the vertical wind shear of the environment, which is calculated using high-resolution model analyses. Afterwards, the accuracy of the parameterization is checked for both motion classes, as well as for classifications according to the lifetime, track length, and severity proxies of the cells. Clear differences between observed and parameterized motion are obtained for all categories, calling for an adjustment of the parameterization in a second step. This adjusted parameterization improves the storm motion estimation for most of the storm categories. A better storm motion estimation improves the calculation of storm-relative helicity, enabling a more reliable nowcasting and forecasting of supercell potential.

Keywords: supercells, Germany, storm-relative helicity, hailstorm, severe convective storms

1 Introduction

Severe convective storms (SCS) and associated phenomena, such as heavy rainfall, large hail, or straight line winds and tornadoes, frequently cause considerable damage to buildings, vehicles, critical infrastructure, and agriculture crops across large parts of Europe (Kunz and Geissbuehler, 2017; Púčik et al., 2019). Over the past two decades, SCS have accounted for about one-third of all losses from natural hazards in Central Europe (MunichRe, 2018), with hail accounting for the largest share. Supercells are the most dangerous convective cells, capable of spawning the largest hailstones, the heaviest rainfall amounts, and the most violent tornadoes (Chisholm and Renick, 1972; Bunkers et al., 2000). Supercells feature a characteristic rotating updraft associated with directional shear in combination with tilting, stretching, and the advection of streamwise vorticity (e.g., Davies-Jones, 1984; Droegemeier et al., 1993; Markowski and Richardson, 2010).

Looking at the occurrence of SCS in Europe in recent decades, we find that six of the ten most expensive hailstorms have occurred in Germany, which makes the country most affected by SCS / hail (Púčik et al., 2019; Allen et al., 2020). Examples of major damaging storms include the two supercells on 27 and 28 July 2013 in central and southern Germany, respectively, with economic losses of around EUR 3.6 billion because of large hail (Kunz et al., 2018); the storm cluster *Ela* on 8–10 July 2014 with economic losses of EUR 2.6 billion mainly in France (SwissRe, 2015) caused by large hail and severe wind gusts (Mathias et al., 2017); and the Munich supercell on 10 July 2019, for which a total loss of almost EUR 1.0 billion (insured loss EUR 0.75 billion) was reported (Munich Re, 2020; Wilhelm et al., 2021). Renewable energy systems (solar, wind turbines), which are currently being substantially expanded in Germany and Europe, are particularly susceptible to SCS (Mishnaevsky Jr et al., 2021; Gupta et al., 2022). The widespread failure of these energy systems can lead to power outages and mid-term power shortages.

Losses from SCS have seen the largest increase of all weather-related perils in Central Europe (Hoeppe, 2016; Púčik et al., 2019). Besides an increase in vulnerable assets in combination with higher susceptibility of modern buildings, the damage increase is at least to a large extent in response to climate change (Raupach et al., 2021). As a result of anthropogenic warming, low-level moisture and convective instability have already increased (Mohr and Kunz, 2013; Rädler et al., 2018; Taszarek et al., 2020a) and are expected to further increase (Mohr et al., 2015; Púčik et al., 2017; Rädler et al., 2019) owing to the Clausius-Clapeyron scaling (O'Gorman and Muller, 2010). Furthermore,

*Corresponding author: Michael Kunz, Institute of Meteorology and Climate Research (IMK-TRO), Karlsruhe Institute of Technology (KIT), Wolfgang-Gaede-Strasse 1, 76131 Karlsruhe, Germany, e-mail: michael.kunz@kit.edu

Gebrüder Borntraeger Science Publishers, Stuttgart, www.borntraeger-cramer.com

it is generally anticipated that simultaneously the melting height will rise, enhancing hailstone melting (Prein and Heymsfield, 2020), whereas vertical wind shear is expected to slightly decrease (Trapp et al., 2007), but with limited influence as it will be overshadowed by the other factors.

Given the large damage associated with SCS, in particular with supercells, and the expected increase in their intensity and frequency in future decades, it is of uttermost importance to better understand their dynamics in order to issue more reliable warnings that potentially can reduce related adverse effects. Despite considerable advances in numerical weather prediction (NWP) models over recent years, the predictability of hailstorms is still very low even by cloud-resolving state-of-the-art numerical weather prediction (NWP) models (Kunz et al., 2018). Main reasons for the limited predictability of thunderstorms are the high nonlinearity of the processes involved in their formation and intensification, their interaction across scales ranging from cloud microphysics over local-scale trigger mechanisms to mesoscale dynamics, and operational observations that usually do not fully cover or resolve convective processes. Nowcasting routines, designed to predict severe weather events for lead times of a few minutes up to one or two hours (e.g., Dixon and Wiener, 1993; James et al., 2018; Hamann et al., 2019), generally have a higher prediction skill compared to purely NWP models as they rely on already observed storms from remote sensing instruments (particularly radar or satellite). Rapidly updating convection-allowing model ensembles, such as the National Severe Storms Laboratory (NSSL) Warn-on-Forecast System (Skinner et al., 2018) or the Seamless INtegrated FOrecastiNg sYstem (SINFONY) of the German Weather Service (Deutscher Wetterdienst, DWD; Ulbrich et al., 2022), skillfully predict storm paths for short lead times, but only if storm signals have been assimilated. Prerequisite for a high prediction skill and high quality of derived warnings, however, are sound estimates of the expected lifetime, intensity and spatial extent of the storms (Zöbisch et al., 2020; Wilhelm et al., in review), as well as the propagation speed and direction. The latter two factors, however, are not easy to determine for supercells because they cannot be derived solely from the ambient wind field.

The dynamics of supercells are largely controlled by dynamic pressure perturbations on the updraft flanks generating vertical pressure gradients extending over a deep layer (Weisman and Klemp, 1982; Rotunno and Klemp, 1985; Bunkers et al., 2000; Markowski and Richardson, 2010). These pressure perturbations can be approximately divided into a linear and nonlinear part. Nonlinear pressure perturbations in an environment with prevailing crosswise vorticity associated with a straight hodograph are responsible for cell splitting, one of the key features of supercells. At the beginning of the cell splitting, a pair of cyclonic and anticyclonic rotation at the flanks of the former updraft forms through tilting of the horizontal vorticity associated with the mean shear (Rotunno and Klemp, 1985; Klemp, 1987). The vortex lines are then tilted downward by a rain-induced downdraft resulting in a downward directed pressure gradient force. The original updraft-centered vortex pair is transformed into two vortex pairs with lifting on both flanks, from which two individual cells develop. In case of a strongly curved hodograph and related streamwise vorticity, cell splitting is rare.

Linear pressure perturbations arise when the updrafts interact with the sheared environment. A dynamic pressure gradient force is directed upwards on the right flank, but downwards on the left flank in cases where the wind turns clockwise with height (Klemp, 1987). As a consequence, this linear forcing leads to a weakening (and dissipation) of the left-moving cell, while the right-moving cell is invigorated. In the case of a counterclockwise hodograph, it is the other way around.

The motion of a supercell can deviate significantly from the (vertically averaged) mean wind (Browning, 1964; Bunkers et al., 2000). Rather the motion is controlled by both the advection of the updraft by the mean wind and the propagation away from the mean wind either toward the right or the left of the shear vector; the latter governed by (linear and nonlinear) dynamic pressure perturbations (Markowski and Richardson, 2010). For storms in the US, it was observed that non-severe thunderstorms moved with a representative mean wind, while stronger, larger, and longer-lived thunderstorms moved slower and to the right of the mean wind (Bunkers et al., 2000). For Europe (France and Germany), Kunz et al. (2020) found that most of the severe hail streaks (diameter > 5 cm) identified from radar data propagated to the right of the mean wind at 500 hPa. An angle difference between 10 and 30° was observed in 35 % of the events, while 21 % had an even larger angle difference.

The propagation of a supercell is determined largely by linear and nonlinear interactions between the updraft and the environmental wind field at different levels, as alluded to above (Davies-Jones, 2002). Different conceptual models (e.g., Fujita and Grandoso, 1968; Rotunno and Klemp, 1985) have attributed the deviation of the storm motion from the mean tropospheric wind to asymmetrically distributed pressure or vertical pressure-gradient forces, which in turn depend on environmental shear. Based on that, several authors have suggested to express the supercell motion either as a function of mean wind speed and direction or with respect to the wind shear vector (e.g., Browning, 1964; Davies and Johns, 1993; Rasmussen and Blanchard, 1998), the latter being preferable because related methods are Galilean invariant (i.e., the relationship between predicted storm motion and the hodograph is independent of the mean wind). A good overview of the different methods is provided by Bunkers et al. (2000). Their proposed and popular method (hereinafter referred to as BU_2000) predicts supercell motion to be 7.5 m s^{-1} perpendicular to the shear vector constructed as the difference between 0–500 m and 5.5–6 km mean wind. This method to predict supercell motion for both right- and left-moving storms was derived and evaluated for a sample of 290 supercell tracks reconstructed from various authors and hodographs from proximity soundings in the United States.

Ambient conditions, particularly prevailing wind shear, instability, and moisture content, however, largely differ between the United States and Europe, mainly because of different geographical features (size and orientation of large mountain chains, local topography). Graf et al. (2011), for example, found from backward trajectories of tornado events that low-level flow blocking by the Alps and the relatively-colder sea surface temperatures over the Atlantic (in contrast to that over the Gulf of Mexico) decisively reduces wind shear and thermodynamic instabilities of tornado environments in Europe. Similar differences in severe storm environments in Europe and the US were analyzed by Taszarek et al. (2020b) and Taszarek et al. (2020c). A less sheared environment and less instability, which reduces the vertical extent of the mesocyclone, in Europe compared to the U.S. may lead to systematic differences in storm motion.

The main objective of our study therefore is to statistically evaluate the skill of the BU_2000 method to predict the motion of supercells in Germany, and to adapt the method by adjusting the parameter values to the observed supercells including both right- and left-movers. Our sample of supercells as well as the analyses are separated into different classes according to specific object characteristics, such as intensity level, length, or lifetime. The adjusted BU_2000 method is used to estimate the impact on the storm-relative helicity (SRH), which was found to outperform deep-layer shear as predictor of SCS (Kunz et al., 2020). An optimization of the motion prediction of supercells is of high relevance for nowcasting purposes as alluded to previously.

For the above described analyses and assessments, three different data sets available for the study area of Germany were combined: (i) tracks of convective cells reconstructed from three-dimensional (3D) radar data using the cell-tracking algorithm TRACE3D (Handwerker, 2002; Schmidberger, 2018); (ii) mesocyclone objects from the radar-based Mesocyclone Detection Algorithm (MCD; Hengstebeck et al., 2018) of DWD; and (iii) assimilation analyses from DWD's formerly operational NWP model COSMO-EU. The cell tracks are used to estimate the storm motion vector. As the focus is on SCS solely, only tracks above a reflectivity of 55 dBZ are considered (Puskeiler et al., 2016; Schmidberger, 2018). The MCD data set allows both to filter supercells from the sample of tracks and to estimate a certain intensity level. With the assimilation analyses hodographs in the vicinity of the storm tracks can be estimated. The study period covers a 4-year period from 2013 to 2016 (April to September), for which all data sets are available. In total 354 supercells were identified homogeneously using the same methods and from uniform data sets (in contrast to BU_2000, who combined SCS tracks from different studies reconstructed by applying different methods).

The paper is structured as follows: Section 2 introduces the methods and data sets used. Section 3 evaluates supercell motion using both the original BU_2000 and an adjusted parameterization, and investigates the differences according to different object classes. The impact of the adjusted parameterization on SRH for all supercells is presented in Section 4. Section 5 finally summarizes the major findings and draws some conclusions.

2 Methods and data

As a short recap, we briefly summarize the most important details of the BU_2000 parameterization first. Afterwards, we describe the different data used in the study at hand, as well as the respective preprocessing and the subsequently following combination of the different data sets.

2.1 Storm motion parameterization

In general, two main atmospheric factors are decisive for the motion of supercells: first, the vertically averaged wind speed and direction determining the advection of the cells, and second the vertical wind shear, which induces the rotation of convective updrafts by vortex-tube tilting of streamwise vorticity. The flanks of the rotating updraft are affected by the dynamic forcing, leading to a deviation of the cell motion direction from the mean (horizontal) wind (e.g., Weisman and Klemp, 1986). As a consequence of the linear pressure perturbations, cells forming a rotating mesocyclone can move right or left with respect to the vertical wind shear vector. Defining it with respect to the vertical wind shear vector, as also done by Bunkers et al. (2000), is more common than with respect to the mean wind. In many cases, a cell moving to the right (left) of the vertical wind shear also moves to the right (left) of the mean wind anyway (Markowski and Richardson, 2010). In the BU_2000 parameterization, the storm motion vector $\boldsymbol{c}$ is therefore parameterized for a right-moving (rm) cell as

$$\boldsymbol{c}_{\mathrm{rm}} = \boldsymbol{v}_{\mathrm{m}} + D\left(\frac{\boldsymbol{v}_{\mathrm{s}} \times \hat{\boldsymbol{k}}}{|\boldsymbol{v}_{\mathrm{s}}|}\right) \tag{2.1}$$

and for a left-moving (lm) supercell as

$$\boldsymbol{c}_{\mathrm{lm}} = \boldsymbol{v}_{\mathrm{m}} - D\left(\frac{\boldsymbol{v}_{\mathrm{s}} \times \hat{\boldsymbol{k}}}{|\boldsymbol{v}_{\mathrm{s}}|}\right). \tag{2.2}$$

Herein, $\boldsymbol{v}_{\mathrm{m}}$ represents the vertically averaged horizontal wind vector and $\boldsymbol{v}_{\mathrm{s}}$ the wind difference between two vertical layers as a measure of vertical wind shear. The parameter D determines the strength of the motion deviation from the mean wind. In order to examine these formulas, Bunkers et al. (2000) used 260 right-moving and 30 left-moving supercells over the contiguous United States. Those cells were partly taken from earlier studies, partly obtained by archived doppler radar data and meteorological literature, and were augmented by video or eyewitness reports. Even though there were supercells where a shallower or thicker layer was more appropriate, the observed motion could be reproduced best, in general, with $\boldsymbol{v}_\mathrm{m}$ as non-pressure-weighted mean wind between 0 and 6 km above ground level (AGL), a parameter value of $D = 7.5\,\mathrm{m\,s^{-1}}$, and $\boldsymbol{v}_\mathrm{s}$ as the 0–0.5 to 5.5–6 km wind shear (AGL). 0–0.5 to 5.5–6 km means, that a mean wind from a 500 m thick layer of that height is used as the lower and upper bounds of the shear vector. In the BU_2000 parameterization, the required environmental data for the computation of the mean wind and vertical wind shear were taken from proximity soundings.

2.2 Data

Three data sets covering the period 2013–2016, with only the warm season (April to September) considered as most of the severe convective storms form during these months in Central Europe, are used in this study to identify supercells over Germany and to examine their motion:

1. Storm tracks objectively obtained from the radar-based cell detection and tracking algorithm TRACE3D (Handwerker, 2002), giving information about potentially hail-producing convective cells;
2. Mesocyclone objects (meso-objects) from the radar-based MCD of DWD, indicating the occurrence of possible supercells (Hengstebeck et al., 2018);
3. Assimilation analyses from DWD's formerly operational NWP model COSMO-EU, which allow a high-resolution assessment of the meteorological ambient conditions such as the wind field (Schulz and Schättler, 2014).

2.2.1 Data preprocessing

The tracking algorithm TRACE3D originally developed by Handwerker (2002) for spherical coordinates utilizes 3D radar reflectivity data from DWD's radar network that are available every 15 minutes, covering Germany and neighbouring regions. Basically, the algorithm performs two steps: first, the detection of a convective cell considering an adaptive threshold method. Based on a first reflectivity threshold, regions of intense precipitation are identified. A second threshold depending on the highest detected reflectivity value within this region is used to determine individual cells that are called reflectivity cores. The second step consists of assigning reflectivity cores from the radar scan 15 minutes before to the cores from the current scan. The algorithm was later adapted by Schmidberger (2018) to cartesian coordinates of the reflectivity data from the DWD radar network. The TRACE3D setup used by Puskeiler et al. (2016) considered a lower threshold value of 55 dBZ irrespective of the height to best identify potentially hail-producing cells. An evaluation of the radar-derived hail days with loss data from a building and an agricultural insurance company confirmed the reliability of the methods and the results. The output of the tracking algorithm TRACE3D are identified potential hail streaks with the geographic center point, the average motion direction ϕ_obs and velocity v_obs, and the length and width of the tracks. When speaking about the lifetime of these objects in the following, this refers to the duration of detection. The real total lifetime (including stages with lower reflectivities) of the associated convective cells is longer.

The MCD utilizes 3D radar-based radial Doppler velocity data with a time resolution of 5 minutes. It searches for high values of positive azimuthal shear, represented by a strong change of radial velocity in the direction of the radar sweep, which are connected with cyclonic rotation (Hengstebeck et al., 2018). Mesoanticyclones are not considered in the algorithm because they are observed less frequently compared to mesocyclones. However, Hengstebeck et al. (2018) mention that mesoanticyclones can often co-occur with cyclonically rotating systems, as in the case of bow echoes with cyclone-anticyclone-couplets, left-movers originating from splitting storms, or supercells with a cyclonically rotating updraft and anticyclonic shear in the midlevels (cf. Section 3.1.1). As a first step of the MCD, pattern vectors are defined as a sequence of positive azimuthal shear. Closely located pattern vectors can be merged into a two-dimensional (2D) feature if they exceed a certain threshold and fulfill a symmetry criterion. These first steps follow basically the pattern vector approach by Zrnic et al. (1985). Afterwards, detected features in different elevations of radar scans can be combined to 3D meso-objects. Depending on their horizontal diameter, vertical extent and maximum azimuthal shear, the meso-objects are classified into different severity levels as shown in Table 1. The MCD provides two diameter measures: the simple diameter, which is defined as the diameter of the largest 2D feature, and the equivalent diameter, which corresponds to the diameter of a circle with the same area as the group of pattern vectors that compose the biggest 2D feature. In contrast to Hengstebeck et al. (2018), we used the diameter instead of the equivalent diameter for the severity classification, because information on the equivalent diameter was rarely available in the data set provided by DWD.

The hourly environmental field data from the NWP model COSMO-EU are originally available on a rotated spherical grid encompassing all of Europe with a grid point distance of 0.0625° (about 7 km; Schulz and Schättler, 2014). These data were rotated to a regular latitude-longitude grid with the zonal and meridional wind components transformed accordingly. On the rotated grid, the surface geopotential as well as the geopotential height and the horizontal wind on different pres-

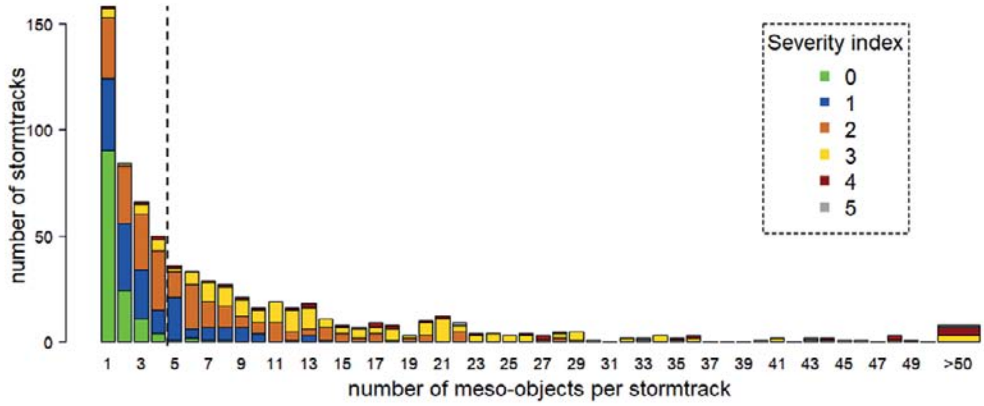

Figure 1: Number of meso-objects per storm track; all tracks with at least five meso-objects (vertical dotted line) are classified as supercells with a specific severity level (colors).

Table 1: Thresholds for classifying meso-objects into different severity levels (Hengstebeck et al., 2018) and number of cells with at least 5 associated meso-objects per severity level. All three conditions must be met for one meso-object to be assigned to the respective severity level.

			severity level					
condition	unit		0	1	2	3	4	5
diameter	km	>	–	3	3	5	5	5
vertical extent	km	>	–	1	2	3	6	8
maximum azimuthal shear	$m\,s^{-1}\,km^{-1}$	>	–	5	7	10	20	30
number of cells			5	53	110	151	31	4

sure levels from 1000 up to 50 hPa were available for the calculation of mean wind and vertical wind shear for input to Eq. (2.1) and (2.2) (Wilhelm, 2022).

2.2.2 Data combination

When combining the data, it is important to consider that the maximum reflectivity and the rotating updraft of a supercell are usually spatially displaced (Markowski and Richardson, 2010). For this reason, we enlarged the TRACE3D track width by 10 km on each side. However, the larger the width, the more often a mesocyclone detected by the MCD can be assigned to a wrong cell. Thus, the 10 km extension applied here is a compromise between incorrect and missed assignments. Only cells which were detected with TRACE3D at least for 5 time steps (75 minutes) were considered, as the typical lifetime of supercells is longer than 1 h (Bunkers et al., 2006; Markowski and Richardson, 2010,).

Due to the high temporal resolution of the radar data, multiple meso-objects from the MCD with different severity levels are assigned to each TRACE3D cell object. Since the highest intensity level throughout the life cycle of the cell is most decisive for the associated potential damage, we considered only the highest level in the subsequent analyses (cf. Table 1). If a track has no or only a few assigned meso-objects, it is assumed not to be a supercell and is sorted out of the sample. According to the frequency distribution of the number of meso-objects assigned to a storm track (Fig. 1), showing a kind of knee at a value of five, this value was set as the lower limit of meso-objects defining a supercell, knowing that a different choice could affect the results (cf. Section 5). This strict filtering may remove some weak supercells from the sample. However, it ensures to a high degree of certainty that the sample consists only of real supercells, which is a prerequisite for the comparison with the BU_2000 parameterization estimating the supercell motion.

After applying the procedure as described above to the 2161 TRACE3D objects, the final supercell data set consists of 354 supercells (16.4 %) over Germany and neighbouring regions (Fig. 2). The corresponding distribution of severity levels is shown in Table 1. Because of low numbers of severity levels 0 (five cells) and 5 (four cells), these are combined with the levels 1 and 4, respectively, for the analyses.

Because the BU_2000 parameterization (Eq. (2.1) and (2.2)) requires information about wind speed and direction at different height levels, we calculated these values from the pressure-level based COSMO-EU wind and geopotential data using a linear interpolation onto equidistant height levels. Because COSMO-EU data are available hourly, we decided to take the values as close as possible to the time of the first cell detection in TRACE3D for the calculation of mean wind and vertical wind shear. If a cell is detected at 30 minutes after the hour, the data from the following hour were taken. For those cells with an early detection of an initial meso-object, this method should work well. For a cell with a long track that contains meso-objects only late in its course, however, other environmental data might be a better choice. Nevertheless, this method is likely to be superior to using proximity soundings. Spatially, we averaged wind and geopotential height across the nine grid points closest to the reconstructed starting coordinate of

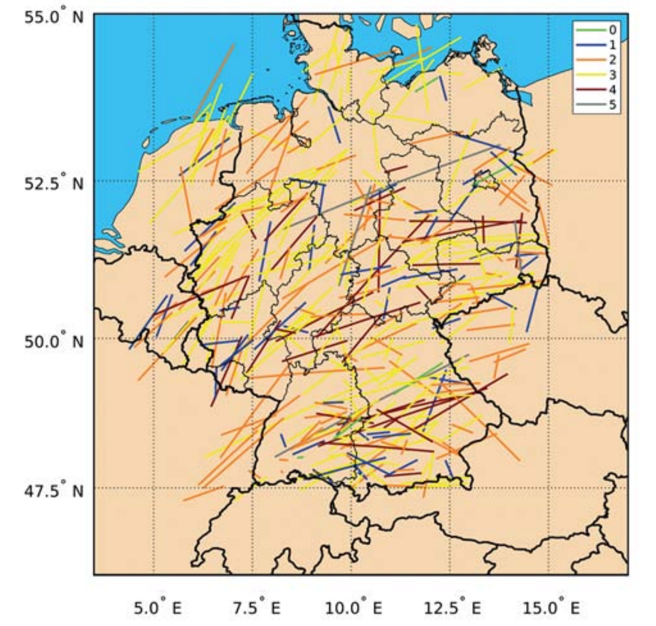

Figure 2: Storm tracks of all 354 supercells identified in the summer half-years (April to September) in the period from 2013 to 2016; colors indicate the highest severity level of the associated meso-objects obtained throughout the life cycle.

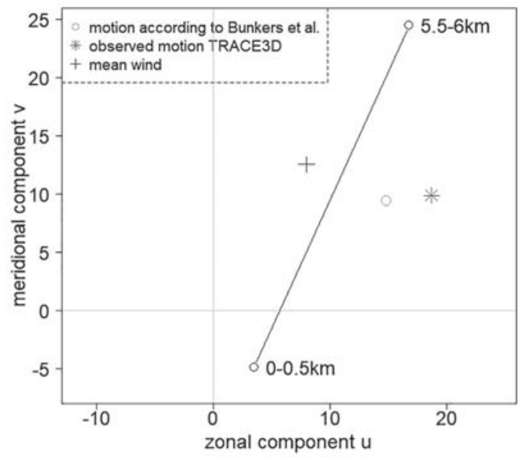

Figure 3: Vertical wind difference (shear) between 0–0.5 km and 5.5–6 km (line), non-pressure-weighted mean wind (+), observed motion from the radar tracking algorithm TRACE3D (*), and computed motion with the BU_2000 parameterization (°) for one exemplaric supercell in southwestern Germany on 28 July 2013 (Kunz et al., 2018). Since the observed motion is on the right side of the vertical wind shear vector, the cell is characterized as a right-moving supercell and the computed motion is to the right of the mean wind on an imaginary line orthogonal to the shear vector.

the cell track, although Potvin et al. (2010) discussed that soundings of too close distance to the storm could be less useful for the storm environment due to convective feedbacks like anvil shadowing or precipitation and found an optimal distance of 40 to 80 km. For the closest 144 grid points (corresponding to an area of about 80 km length), the results in the study at hand are qualitatively very similar to those with only the nine closest grid points (cf. Section 3.1).

After the interpolation of the wind field as described above, a non-pressure-weighted mean wind between 0 and 6 km AGL was calculated in agreement with BU_2000. The same averaging procedure was applied between 5.5 and 6 km, and between 0 and 0.5 km AGL, with their difference providing a measure for the vertical wind shear (deep-layer shear). With this shear vector, it is possible to characterize each cell of the data set as right- or left-moving supercell, considering its corresponding observed average motion direction. Afterwards, the motion of the supercells can be computed using Eq. (2.1) or (2.2). As an example, Fig. 3 shows data of a supercell that caused major damage in southwestern Germany on 28 July 2013 (Kunz et al., 2018). The non-pressure-weighted mean wind and the vertical wind shear of the environment, calculated as described above, can be seen as well as the motion according to the Eq. (2.1). This motion can then be compared with the observed motion via TRACE3D, which by its position to the right of the vertical shear vector causes the cell to be classified as a right-moving supercell.

3 Evaluation of supercell motion

After the preparation of the supercell data set, the differences between parameterized and observed storm motion can be evaluated. Instead of using zonal and meridional components, it is more convenient to express the motion in terms of direction and velocity. To evaluate Eq. (2.1) and (2.2) for supercell motion, the following difference between parameterized and observed direction (ϕ_{BU} and ϕ_{obs}) is used for each cell of the data set:

$$\Delta\tilde{\phi} = \begin{cases} \mathrm{atan2}[\sin(\phi_{\mathrm{BU}} - \phi_{\mathrm{obs}}), \\ \qquad \cos(\phi_{\mathrm{BU}} - \phi_{\mathrm{obs}})] & \text{, for right-moving supercells} \\ -\mathrm{atan2}[\sin(\phi_{\mathrm{BU}} - \phi_{\mathrm{obs}}), \\ \qquad \cos(\phi_{\mathrm{BU}} - \phi_{\mathrm{obs}})] & \text{, for left-moving supercells} \end{cases}, \tag{3.1}$$

with the tilde indicating that $\Delta\tilde{\phi}$ is not the simple direction difference, but the bias of the direction deviation from the mean wind by the parameterization compared to the observed deviation. Thus, a positive $\Delta\tilde{\phi}$ describes either right-moving cells with parameterized direction too far to the right, or left-moving cells too far to the left compared to the observed motion direction. In turn, negative $\Delta\tilde{\phi}$ expresses an underestimation of the direction deviation by the parameterization. The formulation with the atan2 function (according to the R raster package, https://rdocumentation.org/packages/raster/versions/3.5-15, accessed on 22 February 2023) makes sure that the periodicity of the angle coordinate is taken into account.

For the difference between parameterized and observed velocity (v_{BU} and v_{obs}), the velocities are normal-

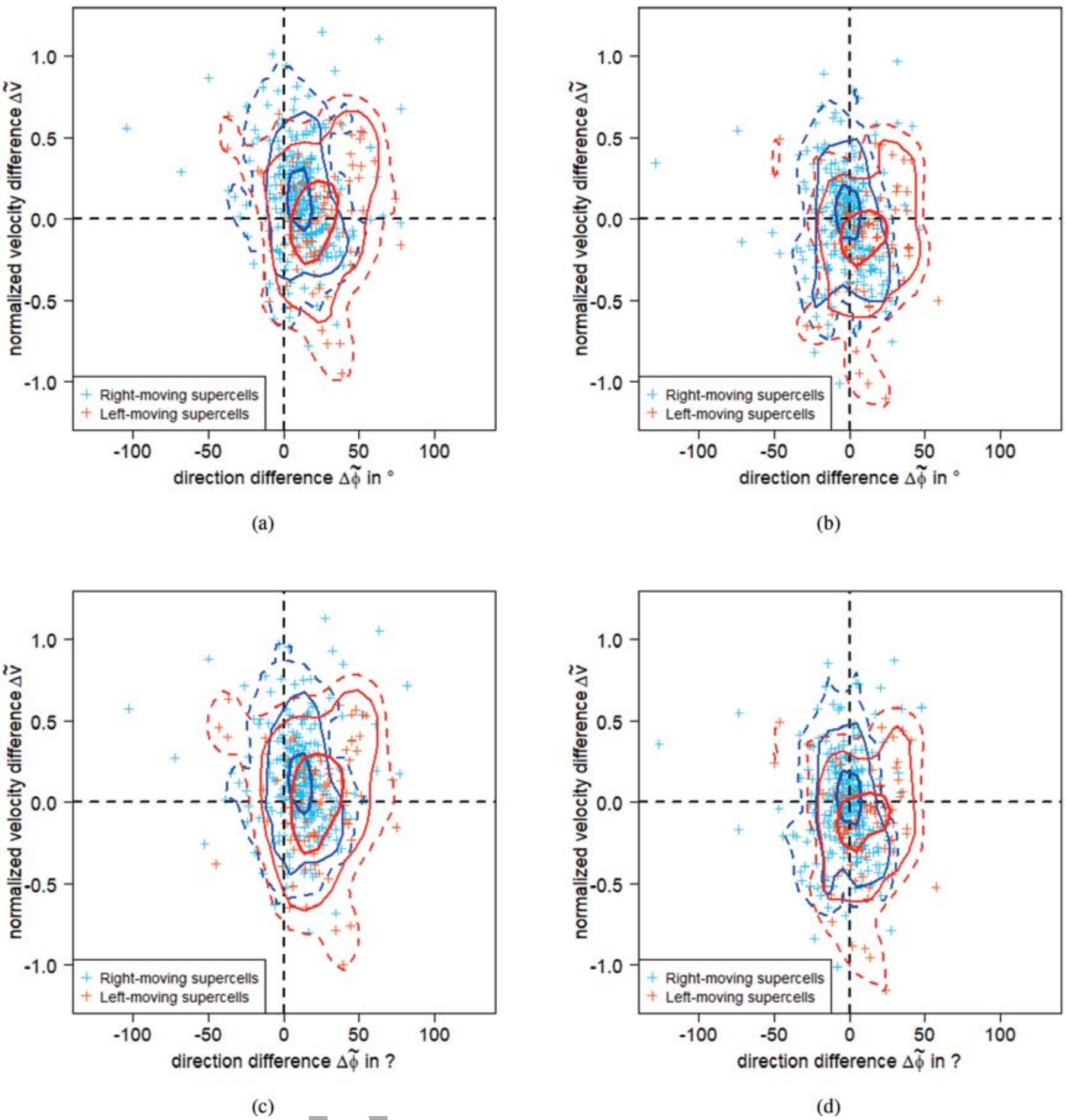

Figure 4: Scatter plots for direction difference $\Delta\tilde{\phi}$ and normalized velocity difference $\Delta\tilde{v}$ for all 354 supercells, separately for right- and left-moving cells, with (a) the BU_2000 parameterization and (b) the BU_4.0 parameterization. (c) is analogous to (a) and (d) to (b) but with using 144 grid points instead of nine for the storm environment. The respective kernel densities (30 sampling points for $\Delta\tilde{\phi} \in [-130°, 130°]$ and $\Delta\tilde{v} \in [-1.2, 1.2]$, respectively) obtained with a Gaussian kernel are displayed with the frequency levels 0.25 (thick solid line), 0.75 (thin solid) and 0.9 (dashed).

ized with their arithmetic mean:

$$\Delta\tilde{v} = \frac{v_{\mathrm{BU}} - v_{\mathrm{obs}}}{0.5 \cdot (v_{\mathrm{BU}} + v_{\mathrm{obs}})} \,. \tag{3.2}$$

The tilde indicates that $\Delta\tilde{v}$ is not the simple motion velocity difference, but rather a normalized dimensionless number, which simplifies the comparison of the individual results of slow- and fast-moving cells by providing a relative measure. It is normalized in the way that values of equal magnitude for $\Delta\tilde{v}$ are obtained when v_{BU} is twice or half as large as v_{obs}. A symmetric normalization only by v_{obs}, where equal magnitude for $\Delta\tilde{v}$ would be obtained for the same increment above or decrement below v_{obs}, was also tested. However, because of fairly similar results and the left-bounded value range of v_{obs}, the normalized velocity difference according to Eq. (3.2) is used in this study.

3.1 Adjustment of the BU_2000 parameterization

3.1.1 Original parameterization

The values of $\Delta\tilde{\phi}$ and $\Delta\tilde{v}$ from Eq. (3.1) and (3.2) for the 354 supercells are evaluated separately for left- and right-moving supercells (Fig. 4). Out of the 354 supercells, 80 are classified as left-moving and 274 right-moving. As mentioned above, the MCD (Hengstebeck et al. 2018) was used by DWD such that only mesocyclones (and no mesoanticyclones) were detected, implying that the majority of storms in the data set moves

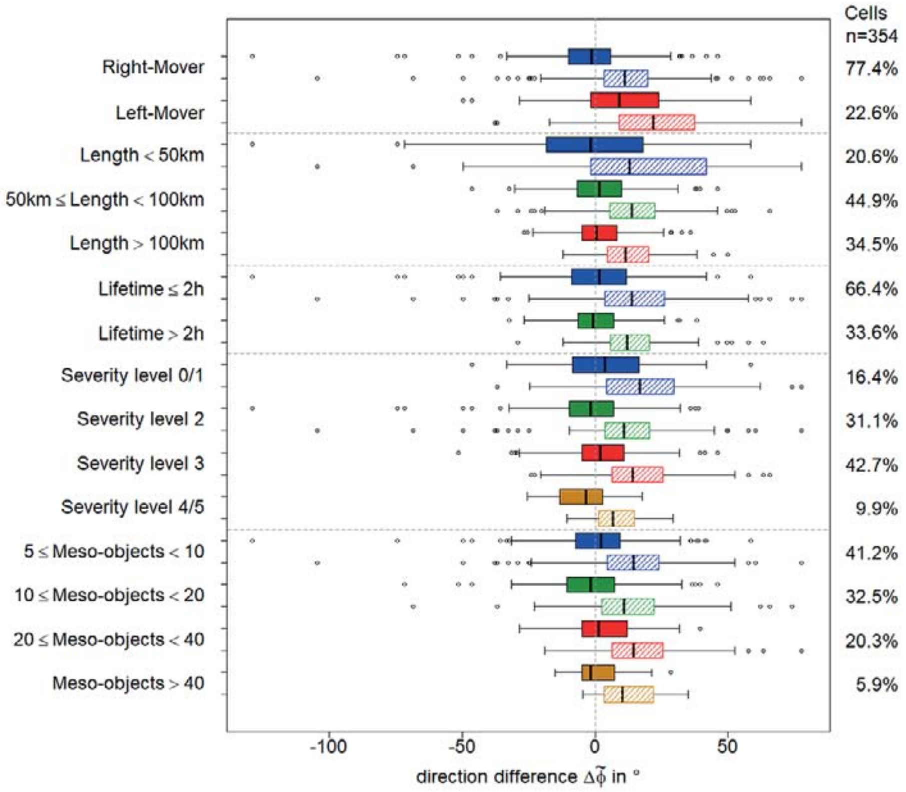

Figure 5: Box- and Whiskers plots for the direction difference $\Delta\tilde{\phi}$ with adjusted parameter $D = 4.0\,\mathrm{m\,s^{-1}}$ (filled boxes) and original parameter $D = 7.5\,\mathrm{m\,s^{-1}}$ (hatched boxes) for all 354 supercells divided into different categories: 1) motion direction, 2) length of storm track, 3) cell lifetime, 4) severity level and 5) number of associated meso-objects. Boxes show the IQR, whiskers outliers up to a deviation of 1.5 IQR. On the right-hand side the respective fraction of cells which contributes to a special category is given.

to the right with respect to the deep-layer shear vector. However, 22.6 % of the cells are left-moving, often coinciding with a partially cyclonal curvature of the hodograph in the lowermost 4 km (Note that the mesocyclone base height mostly ranges between 2 and 4 km AGL).

Fig. 4a shows that the parameterized direction for left-moving supercells is too far to the left and for right-moving cells too far to the right. This is a very clear result because all shown frequency levels of the kernel density estimation (Parzen, 1962), which is used here as a non-parametric way to estimate the underlying parametric probability distribution (Wilks, 2019), are shifted towards the right when using BU_2000, especially the frequency level 0.25, which indicates that the 25 % of supercells within the highest-density region of the data set have overestimated direction deviations. The overestimation appears even more remarkable when viewing at the interquartile range (IQR) of the direction difference for both right- and left-movers, showing that the middle 50 % of the distribution are in the positive range of values (Fig. 5). For the velocity the differences are not as large as for the direction, but a slight overestimation can be seen for both motion directions, especially for the right-moving cells (Fig. 4a and 6). The same overestimation of direction deviation from the mean wind and velocity can be seen when calculating mean wind and shear within a larger proximity of 144 grid points around the storm (Fig. 4c).

3.1.2 Adjusted parameterization

The almost systematic differences between observed and predicted supercell velocity and direction found above make it imperative to adjust the BU_2000 motion parameterization. In order to achieve a rather simple adjustment in the direction estimation, the constant parameter D in Eq. (2.1) and (2.2) is slightly modified. According to the equations, a reduction of D leads, in general, to less deviation of cell motion from the mean wind and therefore to a better direction estimation for the data set. Since $\Delta\tilde{v}$ is too high for both categories, reducing D might also improve the estimation of motion velocity.

The parameter D is systematically reduced with decrements of $0.5\,\mathrm{m\,s^{-1}}$ starting from the original value of $7.5\,\mathrm{m\,s^{-1}}$. For each new D value, direction and velocity as well as the mean absolute error MAE are computed, the latter according to Wilks (2019) via

$$MAE = \frac{1}{n}\sum_{i=1}^{n} |\Delta x_i| \,, \tag{3.3}$$

where $n = 354$ and Δx_i are the direction differences $\Delta\tilde{\phi}$ or normalized velocity differences $\Delta\tilde{v}$, respectively, for each cell. The mean error for the direction difference is smallest for $D = 4.0\,\mathrm{m\,s^{-1}}$ with $MAE = 15.9°$, smaller than for the original value of $D = 7.5\,\mathrm{m\,s^{-1}}$ with

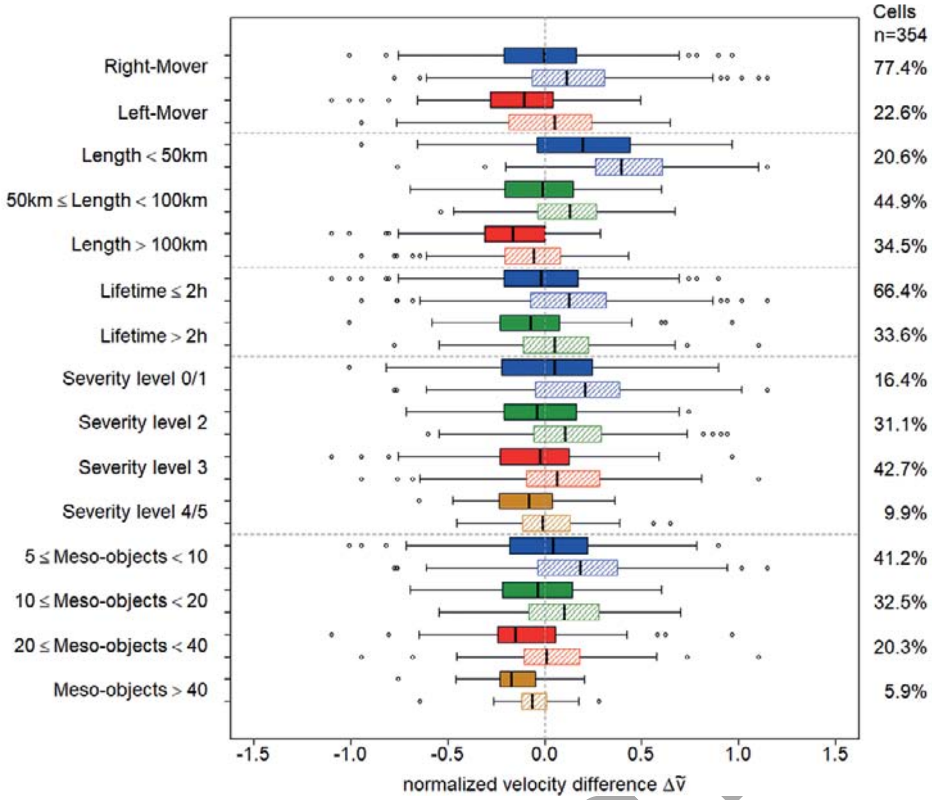

Figure 6: Same plots as in Fig. 5, but for the normalized velocity difference $\Delta\tilde{v}$ instead of direction difference $\Delta\tilde{\phi}$.

$MAE = 21.8°$. For the normalized velocity, the value $D = 3.5\,\mathrm{m\,s^{-1}}$ with $MAE = 0.278$ provides the smallest error, which, however, is only marginally smaller than for $D = 4.0\,\mathrm{m\,s^{-1}}$ with $MAE = 0.279$. Both values show an improvement compared to the original value $D = 7.5\,\mathrm{m\,s^{-1}}$ with $MAE = 0.296$. As a consequence, we decided to adjust the BU_2000 parameterization of supercell motion with $D = 4.0\,\mathrm{m\,s^{-1}}$ in order to achieve the best estimations of storm motion on average. Because it has the same structure as the BU_2000 parameterization, but with a different parameter D, this parameterization is called BU_4.0 in the following. Using the 144 closest grid points leads to slightly different MAE values, but with the same reasoning as above, $D = 4.0\,\mathrm{m\,s^{-1}}$ would be the optimal value for storm motion estimation.

With this adjusted parameter D, the cell motion direction can be estimated well, especially for right-moving supercells. The values of the direction difference $\Delta\tilde{\phi}$ seem to be nearly evenly distributed around zero (Fig. 4b), leading to a median only slightly different from zero (Fig. 5). The estimation of the direction of left-moving supercells is not as good as for right-moving cells, but better than with the BU_2000 parameterization. For the velocity, the estimation is better for right-moving supercells with the BU_4.0 parameterization (Fig. 6). Their IQR is nearly the same as before, but the median of $\Delta\tilde{v}$ is close to zero, what can also be assumed by glancing at the kernel density estimation in Fig. 4b. Only the velocity estimated for left-moving supercells produces larger differences compared to the original D value. In summary, the BU_4.0 parameterization leads to much better results in the estimation of motion for the 274 right-moving supercells, but for the 80 left-moving supercells only in the estimation of direction. Since the results are again very similar for 144 grid points (Fig. 4d), the focus in the following is only on the results for the nine closest grid points representing the storm environment.

3.2 Relations of certain storm track features and motion estimation

Apart from their motion, supercells have several other classifiable features that are of high relevance, for example, with regard to their damage potential (cf. Section 1). These features include the lifetime of the supercell, the length of the storm track, or the number of associated meso-objects and severity levels. In the following, we investigate whether there are systematic differences in the estimation of supercell motion depending on these features. In doing so, we first checked which of the features are correlated. Because the distributions of the different features deviate from the normal distribution, we considered the Spearman rank-correlation coefficient ρ only (Table 2).

The significance level expressed by the p-value is always high enough to indicate statistical significance, with very small p-values ranging from 10^{-16} up to a maximum of $4 \cdot 10^{-4}$. The correlation coefficient shows small to moderate correlations for some features (e.g.,

Table 2: Spearman correlation coefficient ρ and significance level p for different combinations of the supercell features.

feature 1	feature 2	ρ	p
storm track length	lifetime	0.612	$< 2.2 \cdot 10^{-16}$
storm track length	number of meso-objects	0.408	$1.2 \cdot 10^{-15}$
storm track length	severity level	0.281	$7.7 \cdot 10^{-8}$
lifetime	number of meso objects	0.414	$4.5 \cdot 10^{-16}$
lifetime	severity level	0.187	$3.9 \cdot 10^{-4}$
number of meso-objects	severity level	0.578	$< 2.2 \cdot 10^{-16}$

lifetime and severity level). Higher correlations exist between lifetime, storm track length and number of associated meso-objects, whereas the strongest correlation is computed between storm track length and lifetime with $\rho = 0.612$.

3.2.1 Feature relations to direction difference

First, the focus in the analyses is on the direction difference between parameterized and observed direction $\Delta\tilde{\phi}$, which has shown an improvement for the BU_4.0 parameterization (Section 3.1). It is striking that with the original parameter $D = 7.5\,\mathrm{m\,s^{-1}}$ the first quartile is above zero for all features except for cells with a short track of less than 50 km (Fig. 5), indicating a general direction difference overestimation by the BU_2000 parameterization. After the adjustment with $D = 4.0\,\mathrm{m\,s^{-1}}$, the zero value is always within the middle 50 % of the distribution, and the median of the direction difference is closer to zero for all categories. The IQR becomes smaller after the adjustment for all categories except for the most severe cells with severity level 4 and 5.

For the classification with regard to the storm track length, the largest improvement is obtained for cells with long tracks of at least 100 km, for which the IQR is clearly reduced and the median very close to zero. Also for a medium length (at least 50, but less than 100 km) and for short cell tracks (smaller than 50 km), the estimation of the direction is clearly improved compared to the BU_2000 parameterization. Analogous findings are seen for the lifetime of the supercells, as these two categories show the highest correlation (cf. Table 2).

The severity level feature has the smallest correlation with the other features, especially with lifetime and storm track length. For the most severe cells the direction estimation is only marginally improved with the BU_4.0 parameterization. Whereas the median is closer to zero and the zero value is within the middle 50 % of the distribution with the BU_4.0 parameterization, the motion direction is slightly underestimated yielding a somewhat higher IQR. For the least severe cells, in contrast, the direction is still slightly overestimated.

For the analysis of the number of meso-objects assigned to each supercell, the data set is divided into cells with less than 10, at least 10 but less than 20, at least 20 but less than 40 and at least 40 meso-objects. For some of these categories the median is above, for some below, but always closer to zero after adjusting the D parameter. Moreover, the middle 50 % of the distribution narrow for each category.

The results for the categories of the different storm track features show that with the simple adjustment of parameter D, the estimation of the direction can be improved substantially not only for the whole data set but also for many useful supercell classifications. Especially the results for the severity level with an underestimation of storm motion direction for the most severe cells indicate that a separation into different categories or a more sophisticated adjustment might be beneficial for application purposes or subsequent studies. The same applies for the overestimation in the direction for the less severe cells.

3.2.2 Feature relations to velocity difference

For the normalized velocity difference $\Delta\tilde{v}$, the adjustment of the parameterization parameter to $D = 4.0$ turns out to be beneficial for many storm track features, but not for a few others (Fig. 6). Basically for right-moving cells, the change in D leads to a significant improvement in velocity estimation visible at the position of the median and the quartiles. In contrast, a deterioration can be seen for left-moving cells as mentioned above (see also Fig. 4).

For those cells with short or medium track lengths, the median of $\Delta\tilde{v}$ is closer to zero with the BU_4.0 compared to the BU_2000 parameterization, whereas the IQR increases for all categories of cell track length. Nevertheless, for short- and medium track lengths the new setting of D is beneficial, while for long storm tracks the outcome is worse. As could be expected due to the correlation between lifetime and storm track length (cf. Table 2), the velocity estimation can be improved for cells with a lifetime below 2 h, whereas for longer-lasting cells a previous overestimation of the velocity becomes an underestimation visible also at the median.

The findings for the feature categories of the severity level are differing, since the correlation between severity level and storm track length or lifetime, respectively, is small (cf. Table 2). The median again shifts to smaller $\Delta\tilde{v}$ values and is thus closer to zero for the severity levels of 0/1, 2 and 3. For the cells with level 4/5, the results are better with the BU_2000 parameterization. Combining the direction and velocity results for this category, it becomes clear that the adjustment shown in this paper is not beneficial for the motion estimation of the most severe supercells. This is, for example, the case for the supercell shown in Fig. 3 with severity level 5 (Kunz et al., 2018). There it can be seen that a smaller deviation of the parameterized storm motion from the mean wind (smaller D) would result in a higher deviation from the observed motion. Bunkers (2018) and Bunkers et al. (2022) found a farther rightward deviation of tornadic supercells compared with non tornadic ones as well as a faster movement for the tornadic supercells. This is analogous to the results in the present study obtained for the most severe cells with an underestimation of direction deviation and velocity with the adjusted method, and also reasonable under the assumption that more supercells with a high severity level are tornadic than cells that are less severe.

Similar results as for the severity level are obtained for the number of meso-objects, two feature categories which at least show some correlation (cf. Table 2). The adjusted parameterization does not always improve the velocity estimation. For the two categories with the most meso-objects, the adjusted estimates are worse. In contrast to the severity level 4/5 category discussed above, however, the direction difference is considerably better with the adjusted parameter for storm tracks with a large number of meso-objects (cf., Fig. 5).

4 Evaluation of storm-relative helicity

A parameter frequently used in the context of ingredients-based forecasting of severe convective storms that includes the motion vector of these cells is the storm-relative helicity (SRH; e.g., Davies-Jones et al., 1990; Davies and Johns, 1993; Coffer et al., 2019; Kunz et al., 2020). SRH is a measure for vertical wind shear, or more precisely, for the streamwise environmental vorticity available for vortex-tube tilting (Markowski and Richardson, 2010). Due to the influence of the motion direction of the cell, SRH is not Galilean invariant and therefore formulated in the moving reference frame (i.e., relative to the storm movement). According to Markowski and Richardson (2010), SRH can be computed as the vertical integral over a depth of usually $d = 3$ km by multiplying the difference of environmental mean wind $\boldsymbol{v}_\mathrm{m}$ and storm motion vector $\boldsymbol{c}$ with the horizontal vorticity $\boldsymbol{\omega}_\mathrm{h}$:

$$\mathrm{SRH} = \int_0^d (\boldsymbol{v}_\mathrm{m} - \boldsymbol{c}) \cdot \boldsymbol{\omega}_\mathrm{h} \mathrm{d}z\,. \tag{4.1}$$

Here the close relation of SRH to the streamwise (anti-streamwise) vorticity becomes evident. Thus, high SRH absolute values are an important ingredient for the formation and development of right-moving (left-moving) supercells. The SRH is often used to predict the potential of supercell formation in addition to other measures for vertical wind shear, for example, deep-layer shear. For that reason, improving the estimate of supercell motion by an improved parameterization of storm motion $\boldsymbol{c}$ can lead to a better estimate of the potential for supercell formation expressed by SRH.

According to Markowski and Richardson (2010), SRH can be computed via

$$\mathrm{SRH} = \sum_{i=1}^{N-1} = [(u_{i+1} - c_\mathrm{x})(v_i - c_\mathrm{y}) - (u_i - c_\mathrm{x})(v_{i+1} - c_\mathrm{y})], \tag{4.2}$$

when the mean wind with its zonal and meridional components u and v, is present on N pressure layers. Herein, c_x and c_y describe the zonal and meridional components of the motion vector $\boldsymbol{c}$. With the interpolated environmental wind in 10-meter steps from 0 to 3 km derived from COSMO-EU analyses for each of the 354 supercells and the observed motion direction $\boldsymbol{c}_\mathrm{obs}$, the SRH based on $\boldsymbol{c}_\mathrm{obs}$ ($\mathrm{SRH}_\mathrm{obs}$) is calculated using Eq. (4.2). Analogously, using the parameterized motion $\boldsymbol{c}_\mathrm{BU}$ with the original as well as with the adjusted parameter D, the SRH based on the parameterized storm motion is obtained (SRH_BU). Similarly to the differences in motion direction, $\Delta\tilde{\phi}$ and velocity $\Delta\tilde{v}$ (cf. Section 3), a difference of the SRH values between the parameterized and observed motion can be calculated, where the difference results only from the different choice of the motion vector $\boldsymbol{c}$:

$$\Delta\mathrm{SRH} = \mathrm{SRH}_\mathrm{BU} - \mathrm{SRH}_\mathrm{obs}\,. \tag{4.3}$$

From the box plot in Fig. 7a, a clear improvement in the estimation of SRH is visible for the BU_4.0 parameterization compared to the BU_2000, as expected. The SRH differences between observed and estimated motion become smaller, which can be seen from both a smaller median and a smaller IQR. The left-moving supercells are usually accompanied by anti-streamwise vorticity and therefore by negative SRH. Cells in an environment with a mainly clockwise hodograph, but some counterclockwise curvature in the inflow layer, that are classified as left-movers, can be accompanied by positive SRH. The fixed layer for the computation of SRH (0–3 km) can also lead to a different sign than expected for SRH. Therefore one possible improvement could be the computation of an effective SRH over the effective inflow layer of each individual cell as investigated by Thompson et al. (2007). But overall, an estimation of the propagation of a left-moving supercell too far to the left side compared to the mean wind leads to a negative SRH with too high magnitude. For the right-moving supercells accompanied by streamwise vorticity and positive SRH, the estimated propagation too far to the right results in excessive positive values for SRH, even if there are some right-movers with negative SRH for similar reasons as given above for left-movers. The overestimation of SRH magnitude for both left- and right-movers can be seen in Fig. 7b. After the adjustment of the parameterization and a better general estimation of the storm motion $\boldsymbol{c}$, the SRH distribution is narrower and closer to the observed distribution for both left-moving and right-moving cells (Fig. 7c).

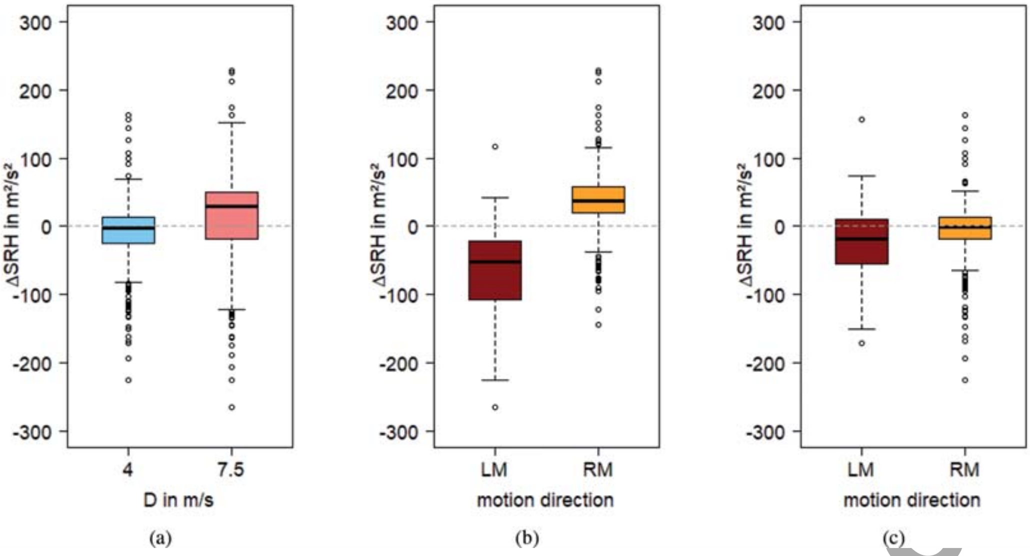

Figure 7: Box plot for ΔSRH for (a) all 354 supercells of the data set, where SRHBU is computed with the motion vector estimated with the adjusted parameter $D = 4.0\,\mathrm{m\,s^{-1}}$ (left) as well as with the original parameter $D = 7.5\,\mathrm{m\,s^{-1}}$ (right). (b)+(c): Distinction between the 80 left-moving and the 274 right-moving supercells of the data set, where SRHBU is computed with the motion vector estimated with (b) original parameter $D = 7.5\,\mathrm{m\,s^{-1}}$ and (c) adjusted parameter $D = 4.0\,\mathrm{m\,s^{-1}}$. Colored boxes show the IQR and include the median which is painted as thicker black line, whiskers reach to the values within a range of 1.5 IQR.

5 Conclusions

In our study, we have statistically evaluated and adjusted the BU_2000 method for predicting the movement of supercells for a large sample comprising 354 events over a four-year period in Germany. The combination of SCS tracks derived from 3D radar data to determine the storm motion vector with data from the radar-based MCD of DWD made it possible to filter out all non-rotating cell objects. The resulting sample of events comprising only rotating supercells was further separated into different object classes with respect to their severity level, track length, and lifetime. The cell objects were additionally combined with COSMO-EU assimilation analyses to estimate hodographs in the vicinity of the storm tracks. The adjusted BU_2000 method was also used to estimate the impact of the changes on the SRH for the entire supercell sample. An optimization of the motion prediction of supercells is of high relevance for nowcasting purposes and the issuing of warnings. Our main goal in the study was to improve the prediction of supercell motion by a simple adaptation of the BU_2000 method, but not to fundamentally change the method as it is best known and widely used.

The following conclusions can be drawn from our research:

- The original BU_2000 method computed for the entire sample of supercells predicts a motion direction that is too far to the left for left-moving cells and too far to the right for right-movers. For the velocity prediction, the result is not as clear, but a slight velocity overestimation can be seen for both motion directions, which is slightly more distinct for the right-moving cells.
- The best agreement between the parameterized and observed motion is obtained for an adjusted parameter of $D = 4.0\,\mathrm{m\,s^{-1}}$ (instead of $D = 7.5\,\mathrm{m\,s^{-1}}$ in the original BU_2000 version). This finding applies to both the entire sample of supercells, but also when separating between right- and left-movers, with the largest improvement for the motion direction.
- The results for the different object categories (track length, lifetime, severity level, number of meso-objects) reveal that with the simple adjustment of the parameter D, the estimation of the direction can be improved not only for the whole data set, but also for most of the categories. Especially the results for the most severe cells according to the severity level (yielding an underestimation of storm motion direction and velocity) indicate that a separation into different categories or a more sophisticated adjustment might be beneficial for application purposes or subsequent studies.
- Different results for different numbers of meso-objects per storm track indicate the sensitivity to the supercell detection criteria. The threshold for meso-objects assigned to a storm track was not set below five objects, in order to prevent too many non-supercells from being classified as supercells. How a different choice for this threshold, or for the threshold in radar reflectivity of the tracking algorithm, or a different MCD would affect the results and the optimal D value, would be interesting to look at in future studies.

- Improving the estimate of the supercell motion by an improved parameterization of the storm motion vector ***c*** led to a better estimate of the supercell potential expressed by SRH for both left- and right-moving storms, which would be beneficial for a forecaster.
- For an improvement of area-based severe weather warnings, an estimation of the movement direction (= affected areas) as accurate as possible is more important than an accurate velocity forecast (= exact timing of severe weather). Even though also the velocity was slightly improved, the strong improvement in the direction estimation is already a good reason to use our adapted parameterization operationally.

Discrepancies between Bunkers et al. (2000) and our study arise for several reasons: (i) Bunkers et al. (2000) used proximity soundings with limited spatial and temporal resolutions with the goal "to obtain a representative background vertical wind shear profile of the supercell environment and not a tornado/supercell proximity sounding". In our study, the hodographs were computed from NWP model analyses at the first detection of the cell and not during the most intense supercell phase as claimed in Bunkers et al. (2000). In general, assigning a cell to a representative environment is a challenging task. The use of NWP model analyses with high spatial and temporal resolution (approx. 7 km and 1 hour), however, provides a reliable assignment between tracks and wind fields, that could easily be adopted in nowcasting procedures with NWP forecasts. For cells with an early detection of a first meso-object according to the MCD, the proposed method should fit well. For longer tracks, which contain meso-objects only later during their course, however, the hodographs and the supercell could be more displaced spatially and temporally. When testing the effect of convective feedbacks in the NWP analyses by using a larger area for representing the storm environment, no qualitative changes of the results can be reported. (ii) Bunkers et al. (2000) combined different data sets (tracks and hodographs) reconstructed by different methods. The methods used in our study remained the same for the entire sample of events. (iii) As already discussed in the introduction, supercell environments in the USA tend to be dominated by a higher wind shear compared to European environments. This may at least partly explain the differences of the optimal D value and the smaller value for Germany.

We found that the hodographs in some cases are very complex, sometimes with clockwise or counterclockwise directions over confined layers. Therefore, distinguishing between right- and left-moving cells from the hodograph is very sensitive to the layers considered to calculate the shear. For a follow-up study it would make sense not to rely strictly on the 0–6 km deep-layer shear, but rather to flexibly adjust the shear estimation to a given hodograph. Finally, concerning the MCD algorithm, we found in our sample a few events with counterclockwise hodograph and associated left-moving supercells. Therefore, we would suggest not to restrict this algorithm to cyclonic rotation, but to allow for antiycyclonic rotation.

Acknowledgments

We would like to express our sincere thanks to Manuel Schmidberger (KIT) for the provision of the radar-based tracks of SCS. DWD is acknowledged for providing mesocyclone objects from the radar-based Mesocyclone Detection Algorithm. COSMO-EU model simulations were performed in the frame of a project funded by the German Federal Ministry for Transport and Digital Infrastructure (BMVI; administrative number Z30/SeV/288.3/1582/LF16). We acknowledge support by the KIT-Publication Fund of the Karlsruhe Institute of Technology.

References

Allen, J.T., I.M. Giammanco, M.R. Kumjian, H.J. Punge, Q. Zhang, P. Groenemeijer, M. Kunz, K. Ortega, 2020: Understanding hail in the earth system. – Rev. Geophys. **58**, e2019RG000665, DOI: 10.1029/2019RG000665.

Browning, K.A., 1964: Airflow and precipitation trajectories within severe local storms which travel to the right of the winds. – J. Atmos. Sci. **6**, 634–639, DOI: 10.1175/1520-0469(1964)021<0634:AAPTWS>2.0.CO;2.

Bunkers, M.J., 2018: Observations of right-moving supercell motion forecast errors. – Wea. Forecast. **1**, 145–159, DOI: 10.1175/WAF-D-17-0133.1.

Bunkers, M.J., B.A. Klimowski, J.W. Zeitler, R.L. Thompson, M.L. Weisman, 2000: Predicting supercell motion using a new hodograph technique. – Wea. Forecast. **15**, 61–79, DOI: 10.1175/1520-0434(2000)015<0061:PSMUAN>2.0.CO;2.

Bunkers, M.J., M.R. Hjelmfelt, P.L. Smith, 2006: An observational examination of long-lived supercells. part i: Characteristics, evolution, and demise. – Wea. Forecast. **5**, 673–688, DOI: 10.1175/WAF949.1.

Bunkers, M.J., M.B. Wilson, M.S. Van Den Broeke, D.J. Healey, 2022: Scan-by-scan storm-motion deviations for concurrent tornadic and nontornadic supercells. – Wea. Forecast. **5**, 749–770, DOI: 10.1175/WAF-D-21-0153.1.

Chisholm, A.J., J.H. Renick, 1972: The kinematics of multicell and supercell Alberta hailstorms. – Alberta Hail Studies Rep. **72-2, 24-31**, 53 pp.

Coffer, B.E., M.D. Parker, R.L. Thompson, B.T. Smith, R.E. Jewell, 2019: Using near-ground storm relative helicity in supercell tornado forecasting. – Wea. Forecast. **5** 1417–1435, DOI: 10.1175/WAF-D-19-0115.1.

Davies, J.M., R.H. Johns, 1993: Some Wind and Instability Parameters Associated With Strong And Violent Tornadoes: 1. Wind Shear And Helicity. – In: The Tornado: Its Structure, Dynamics, Prediction, and Hazards, 573–582. – Amer. Geophys. Union.

Davies-Jones, R., 1984: Streamwise vorticity: The origin of updraft rotation in supercell storms. – J. Atmos. Sci. **41**, 2991–3006, DOI: 10.1175/1520-0469(1984)041<2991:SVTOOU>2.0.CO;2.

Davies-Jones, R., 2002: Linear and nonlinear propagation of supercell storms. – J. Atmos. Sci. **22**, 3178–3205, DOI: 10.1175/1520-0469(2003)059<3178:LANPOS>2.0.CO;2.

Davies-Jones, R., D. Burgess, M. Foster, 1990: Test of helicity as a tornado forecast parameter. – In: Preprints 16th Conf. on Severe Local Storms, Kananaskis Park, AB, Canada, 1990, 588–592. Amer. Meteor. Soc.

Dixon, M., G. Wiener, 1993: TITAN: Thunderstorm identification, tracking, analysis, and nowcasting – A radar-based methodology. – J. Atmos. Ocean. Technol. **10**, 785–797, DOI: 10.1175/1520-0426(1993)010<0785:TTITAA>2.0.CO;2.

Droegemeier, K.K., S.M. Lazarus, R. Davies-Jones, 1993: The influence of helicity on numerically simulated convective storms. – Mon. Wea. Rev. **121**, 2005–2029, DOI: 10.1175/1520-0493(1993)121<2005:TIOHON>2.0.CO;2.

Fujita, T., H. Grandoso, 1968: Split of a thunderstorm into anticyclonic and cyclonic storms and their motion as determined from numerical model experiments. – J. Atmos. Sci. **3**, 416–439.

Graf, M.A., M. Sprenger, R.W. Moore, 2011: Central European tornado environments as viewed from a potential vorticity and Lagrangian perspective. – Atmos. Res. **101**, 31–45, DOI: 10.1016/j.atmosres.2011.01.007.

Gupta, V., M. Sharma, R. Pachauri, K.D. Babu, 2022: Impact of hailstorm on the performance of pv module: a review. – Energy Sources, Part A: Recovery, Utilization, and Environmental Effects (1), 1923–1944, DOI: 10.1080/15567036.2019.1648597.

Hamann, U., J. Zeder, L. Beusch, L. Clementi, L. Foresti, A. Hering, D. Nerini, L. Nisi, M. Sassi, U. Germann, 2019: Nowcasting of thunderstorm severity with Machine Learning in the Alpine Region. – 3rd European Nowcasting Conference, Madrid, Spanien. URL: https://repositorio.aemet.es/handle/20.500.11765/10617 (accessed on 22 February 2023).

Handwerker, J., 2002: Cell tracking with TRACE3D – A new algorithm. – Atmos. Res. **31**, 15–34, DOI: 10.1016/S0169-8095(01)00100-4.

Hengstebeck, T., K. Wapler, D. Heizenreder, P. Joe, 2018: Radar Network-Based Detection of Mesocyclones at the German Weather Service. – J. Atmos. Ocean. Technol. **35**, 299–321, DOI: 10.1175/JTECH-D-16-0230.1.

Hoeppe, P., 2016: Trends in weather related disasters – Consequences for insurers and society. – Wea. Climate Extrem. **11**, 70–79, DOI: 10.1016/j.wace.2015.10.002.

James, P.M., B.K. Reichert, D. Heizenreder, 2018: NowCastMIX: Automatic integrated warnings for severe convection on nowcasting time scales at the German Weather Service. – Wea. Forecast. **33**, 1413–1433, DOI: 10.1175/WAF-D-18-0038.1.

Klemp, J.B., 1987: Dynamics of tornadic thunderstorms. – Annu. Rev. Fluid. Mech. **19**, 369–402, DOI: 10.1146/annurev.fl.19.010187.002101.

Kunz, M., P. Geissbuehler, 2017: Natural Catastrophe Risk Management and Modelling. A Practitioner's Guide, chapter 3.4 Severe Convective Storms. – Wiley Blackwell, 209–217.

Kunz, M., U. Blahak, J. Handwerker, M. Schmidberger, H.J. Punge, S. Mohr, E. Fluck, K.M. Bedka, 2018: The severe hailstorm in southwest Germany on 28 July 2013: characteristics, impacts and meteorological conditions. – Quart. J. Roy. Meteor. Soc. **144**, 231–250, DOI: 10.1002/qj.3197.

Kunz, M., J. Wandel, E. Fluck, S. Baumstark, S. Mohr, S. Schemm, 2020: Ambient conditions prevailing during hail events in central Europe. – Nat. Hazards Earth Syst. Sci. **20**, 1867–1887, DOI: 10.5194/nhess-20-1867-2020.

Markowski, P., Y. Richardson, 2010: Mesoscale Meteorology in Midlatitudes. – John Wiley & Sons, Ltd., Publication, Chichester, Vereinigtes Königreich.

Mathias, L., V. Ermert, F.D. Kelemen, P. Ludwig, J.G. Pinto, 2017: Synoptic analysis and hindcast of an intense bow echo in Western Europe: The 9 June 2014 storm. – Wea. Forecast. **3**, 1121–1141, DOI: 10.1175/WAF-D-16-0192.1.

Mishnaevsky Jr, L., C.B. Hasager, C. Bak, A.M. Tilg, J.I. Bech, S.D. Rad, S. Fæster, 2021: Leading edge erosion of wind turbine blades: Understanding, prevention and protection. – Renew. Energy **169**, 953–969, DOI: 10.1016/j.renene.2021.01.044.

Mohr, S., M. Kunz, 2013: Recent trends and variabilities of convective parameters relevant for hail events in Germany and Europe. – Atmos. Res. **123**, 213–228, DOI: 10.1016/j.atmosres.2012.05.016.

Mohr, S., M. Kunz, K. Keuler, 2015: Development and application of a logistic model to estimate the past and future hail potential in Germany. – J. Geophys. Res. **120**, 3939–3956, DOI: 10.1002/2014JD022959.

Munich Re, 2020: Medieninformationen, Münchener Rückversicherungs-Gesellschaft, München, Deutschland. – URL: https://www.munichre.com/de/unternehmen/media-relations/medieninformationen-und-unternehmensnachrichten/medieninformationen/2020/milliardenschaeden-praegen-bilanz-naturkatastrophen-2019.html#1480610047 (accessed on 22 February 2023).

MunichRe, 2018: NatCatSERVICE – The natural catastrophe loss database. – https://www.munichre.com/en/solutions/for-industry-clients/natcatservice.html.

O'Gorman, P., C.J. Muller, 2010: How closely do changes in surface and column water vapor follow clausius-clapeyron scaling in climate change simulations? – Env. Res. Lett. **2**, 025207, DOI: 10.1088/1748-9326/5/2/025207.

Parzen, E., 1962: On estimation of a probability density function and mode. – Annals Math. Stat. **33**, 1065–1076, DOI: 10.1214/aoms/1177704472.

Potvin, C.K., K.L. Elmore, S.J. Weiss, 2010: Assessing the impacts of proximity sounding criteria on the climatology of significant tornado environments. – Wea. Forecast. **3**, 921–930, DOI: 10.1175/2010WAF2222368.1.

Prein, A.F., A.J. Heymsfield, 2020: Increased melting level height impacts surface precipitation phase and intensity. – Nat. Climate Change **8**, 771–776, DOI: 10.1038/s41558-020-0825-x.

Púčik, T. P. Groenemeijer, A.T. Rädler, L. Tijssen, G. Nikulin, A.F. Prein, van E. Meijgaard, R. Fealy, D. Jacob, C. Teichmann, 2017: Future changes in European severe convection environments in a regional climate model ensemble. – J. Climate **17**, 6771–6794, DOI: 10.1175/JCLI-D-16-0777.1.

Púčik, T., C. Castellano, P. Groenemeijer, T. Kühne, A.T. Rädler, B. Antonescu, E. Faust, 2019: Large Hail Incidence and Its Economic and Societal Impacts across Europe. – Mon. Wea. Rev. **147**, 3901–3916, DOI: 10.1175/MWR-D-19-0204.1.

Puskeiler, M., M. Kunz, M. Schmidberger, 2016: Hail statistics for Germany derived from single-polarization radar data. – Atmos. Res. **178–179**, 459–470, DOI: 10.1016/j.atmosres.2016.04.014.

Rasmussen, E.N., D.O. Blanchard, 1998: A Baseline Climatology of Sounding-Derived Supercell andTornado Forecast Parameters. – Wea. Forecast. **13**, 1148–1164, DOI: 10.1175/1520-0434(1998)013<1148:ABCOSD>2.0.CO;2.

Raupach, T.H., O. Martius, J.T. Allen, M. Kunz, S. Lasher-Trapp, S. Mohr, K.L. Rasmussen, R.J. Trapp, Q. Zhang, 2021: The effects of climate change on hailstorms. – Nat. Rev. Earth Env. **2**, 213–226, DOI: 10.1038/s43017-020-00133-9.

Rotunno, R., J. Klemp, 1985: On the rotation and propagation of simulated supercell thunderstorms. – J. Atmos. Sci. **42**, 271–292, DOI: 10.1175/1520-0469(1985)042<0271:OTRAPO>2.0.CO;2.

Rädler, A.T., P. Groenemeijer, E. Faust, R. Sausen, 2018: Detecting severe weather trends using an additive regressive convective hazard model (AR-CHaMo). – J. Appl. Meteor. Climatol. **3**, 569–587, DOI: 10.1175/JAMC-D-17-0132.1.

Rädler, A.T., P.H. Groenemeijer, E. Faust, R. Sausen, T. Púčik, 2019: Frequency of severe thunderstorms across Europe expected to increase in the 21st century due to rising instability. – npj Climate Atmos. Sci. **30**, DOI: 10.1038/s41612-019-0083-7.

Schmidberger, M., 2018: Hagelgefährdung und Hagelrisiko in Deutschland basierend auf einer Kombination von Radardaten und Versicherungsdaten. – Wissenschaftliche Berichte des Instituts für Meteorologie und Klimaforschung des Karlsruher Instituts für Technologie (KIT), **78**, KIT Scientific Publishing, Karlsruhe, Germany.

Schulz, J.P., U. Schättler, 2014: Kurze Beschreibung des Lokal-Modells Europa COSMO-EU (LME) und seiner Datenbanken auf dem Datenserver des DWD. Deutscher Wetterdienst, Offenbach, Deutschland. – https://www.dwd.de/SharedDocs/downloads/DE/modelldokumentationen/nwv/cosmo_eu/cosmo_eu_dbbeschr_201406.pdf?__blob=publicationFile&v=3 (accessed on 22 February 2023).

Skinner, P.S., D.M. Wheatley, K.H. Knopfmeier, A.E. Reinhart, J.J. Choate, T.A. Jones, G.J. Creager, D.C. Dowell, C.R. Alexander, T.T. Ladwig, others, 2018: Object-based verification of a prototype warn-on-forecast system. – Wea. Forecast. **5**, 1225–1250, DOI: 10.1175/WAF-D-18-0020.1.

SwissRe, 2015: 'Sigma - Natural catastrophes and man-made disasters in 2014: convective and winter storms generate most losses'. Technical report, Swiss Re Economic Research and Consulting Zurich, Switzerland. – https://www.swissre.com/institute/research/sigma-research/sigma-2015-02.html (accessed on 22 February 2023).

Taszarek, M., J.T. Allen, H.E. Brooks, N. Pilguj, B. Czernecki, 2020a: Differing trends in united states and european severe thunderstorm environments in a warming climate. – Bull. Amer. Meteor. Soc. **102**, E296–E322, DOI: 10.1175/BAMS-D-20-0004.1.

Taszarek, M., J.T. Allen, P. Groenemeijer, R. Edwards, H.E. Brooks, V. Chmielewski, S.E. Enno, 2020b: Severe convective storms across Europe and the United States. Part I: Climatology of lightning, large hail, severe wind, and tornadoes. – J. Climate **33**, 10239–10261, DOI: 10.1175/JCLI-D-20-0345.1.

Taszarek, M., J.T. Allen, T. Púčik, K.A. Hoogewind, H.E. Brooks, 2020c: Severe convective storms across Europe and the United States. Part II: ERA5 environments associated with lightning, large hail, severe wind, and tornadoes. – J. Climate **33**, 10263–10286, DOI: 10.1175/JCLI-D-20-0346.1.

Thompson, R.L., C.M. Mead, R. Edwards, 2007: Effective storm-relative helicity and bulk shear in supercell thunderstorm environments. – Wea. Forecast. **1**, 102–115, DOI: 10.1175/WAF969.1.

Trapp, R.J., N.S. Diffenbaugh, H.E. Brooks, M.E. Baldwin, E.D. Robinson, J.S. Pal, 2007: Changes in severe thunderstorm environment frequency during the 21st century caused by anthropogenically enhanced global radiative forcing. – Proc. Natl. Acad. Sci. **50**, 19719–19723, DOI: 10.1073/pnas.0705494104.

Ulbrich, S., C. Welzbacher, T. Hanisch, R. Potthast, U. Blahak, 2022: Rapid update cycle in dwd's seamless integrated forecasting system (sinfony). – Technical report, EMS Annual Meeting 2022, Bonn, Germany, 5–9 Sep 2022, EMS2022-308.

Weisman, M.L., J.B. Klemp, 1982: The dependence of numerically simulated convective storms on vertical wind shear and buoyancy. – Mon. Wea. Rev. **6**, 504–520, DOI: 10.1175/1520-0493(1982)110<0504:TDONSC>2.0.CO;2.

Weisman, M.L., J.B. Klemp, 1986: Characteristics of isolated convective storms. – In: Mesoscale meteorology and forecasting, Springer, 331–358.

Wilhelm, J., 2022: Einfluss atmosphärischer Umgebungsbedingungen auf den Lebenszyklus konvektiver Zellen in der Echtzeit-Vorhersage. – Wissenschaftliche Berichte des Instituts für Meteorologie und Klimaforschung des Karlsruher Instituts für Technologie (KIT), **85**, KIT Scientific Publishing, Karlsruhe, Germany.

Wilhelm, J., S. Mohr, H.J. Punge, B. Mühr, M. Schmidberger, J.E. Daniell, K.M. Bedka, M. Kunz, 2021: Severe thunderstorms with large hail across Germany in June 2019. – Weather **76**, 228–237, DOI: 10.1002/wea.3886.

Wilhelm, J., K. Wapler, U. Blahak, R. Potthast, M. Kunz, in review: Statistical relevance of meteorological ambient conditions for nowcasting the life cycle of convective storms. – Quart. J. Roy. Meteor. Soc.

Wilks, D.S., 2019: Statistical Methods in the Atmospheric Sciences. – Elsevier, Amsterdam, Niederlande.

Zöbisch, I., C. Forster, T. Zinner, L. Bugliaro, A. Tafferner, K. Wapler, 2020: Characteristics of deep moist convection over Germany in multi-source data. – Meteorol. Z. **29**, 393–407, DOI: 10.1127/metz/2020/1011.

Zrnić, D., D. Burgess, L. Hennington, 1985: Automatic detection of mesocyclonic shear with doppler radar. – J. Atmos. Ocean. Technol. **4**, 425–438, DOI: 10.1175/1520-0426(1985)002<0425:ADOMSW>2.0.CO;2.